NMR Structure of Free RGS4 Reveals an Induced Conformational Change upon Binding Gα‡

Franklin J. Moy,§ Pranab K. Chanda,|| Mark I. Cockett,|| Wade Edris,|| Philip G. Jones,|| Kim Mason,§ Simon Semus,§ and Robert Powers*,§

Departments of Biological Chemistry and Neurosciences, Wyeth Research, 85 Bolton Street, Cambridge, Massachusetts 02140

Received December 2, 1999; Revised Manuscript Received April 10, 2000

ABSTRACT: Heterotrimeric guanine nucleotide-binding proteins (G-proteins) are transducers in many cellular transmembrane signaling systems where regulators of G-protein signaling (RGS) act as attenuators of the G-protein signal cascade by binding to the Gα subunit of G-proteins ($G_{i\alpha1}$) and increasing the rate of GTP hydrolysis. The high-resolution solution structure of free RGS4 has been determined using two-dimensional and three-dimensional heteronuclear NMR spectroscopy. A total of 30 structures were calculated by means of hybrid distance geometry−simulated annealing using a total of 2871 experimental NMR restraints. The atomic rms distribution about the mean coordinate positions for residues 5−134 for the 30 structures is 0.47 ± 0.05 Å for the backbone atoms, 0.86 ± 0.05 Å for all atoms, and 0.56 ± 0.04 Å for all atoms excluding disordered side chains. The NMR solution structure of free RGS4 suggests a significant conformational change upon binding $G_{i\alpha1}$ as evident by the backbone atomic rms difference of 1.94 Å between the free and bound forms of RGS4. The underlying cause of this structural change is a perturbation in the secondary structure elements in the vicinity of the $G_{i\alpha1}$ binding site. A kink in the helix between residues K116−Y119 is more pronounced in the RGS4−$G_{i\alpha1}$ X-ray structure relative to the free RGS4 NMR structure, resulting in a reorganization of the packing of the N-terminal and C-terminal helices. The presence of the helical disruption in the RGS4−$G_{i\alpha1}$ X-ray structure allows for the formation of a hydrogen-bonding network within the binding pocket for $G_{i\alpha1}$ on RGS4, where RGS4 residues D117, S118, and R121 interact with residue T182 from $G_{i\alpha1}$. The binding pocket for $G_{i\alpha1}$ on RGS4 is larger and more accessible in the free RGS4 NMR structure and does not present the preformed binding site observed in the RGS4−$G_{i\alpha1}$ X-ray structure. This observation implies that the successful complex formation between RGS4 and $G_{i\alpha1}$ is dependent on *both* the formation of the bound RGS4 conformation and the proper orientation of T182 from $G_{i\alpha1}$. The observed changes for the free RGS4 NMR structure suggest a mechanism for its selectivity for the Gα−GTP−Mg^{2+} complex and a means to facilitate the GTPase cycle.

A ubiquitous component of signal transduction pathways is a heterotrimeric guanine nucleotide-binding protein (G-protein)[1] coupled to a cell surface receptor (for reviews see refs *1*−*4*). G-proteins relay signals initiated by photons, odorants, and a number of hormones and neurotransmitters where a variety of diseases are caused by defects in G-protein activity. The structure of the G-protein is composed of an α-subunit (Gα) that is associated with both the intracellular carboxy-terminal tail of a seven-helical transmembrane receptor and weakly bound to a dimer (Gβγ) of a β-subunit tightly bound to a γ-subunit. G-proteins transfer signals from more than 1000 receptors where various Gα subtypes regulate a variety of distinct downstream signaling pathways and the guanine nucleotide binding, and GTPase function within the Gα domain regulates the activity of G-proteins.

The G-protein signaling process is typically initiated by the binding of an agonist to the cell surface receptor, resulting in an induced conformational change in the G-protein. The G-protein structural change affects the guanine nucleotide affinity of Gα where it preferentially binds GTP and Mg^{2+} over GDP. Numerous X-ray structures for $G_{i\alpha1}$ during the various stages of the GTPase cycle have identified regions of induced conformational changes (*5*−*8*). In particular, the Gα guanine nucleotide-binding site is composed of three distinct "switch" regions: residues V179−V185 in switch I, residues Q204−H213 in switch II, and residues A235−N237 in switch III, which undergo conformational changes

‡ Atomic coordinates for the 30 final simulated annealing structures and the restrained minimized mean structure of RGS4 have been deposited in the Brookhaven Protein Data Bank (codes 1ezy and 1ezt).

* Corresponding author. Telephone: (617)-665-7997. Fax: (617)-665-8993. E-mail: powersr@war.wyeth.com.

§ Department of Biological Chemistry.

|| Department of Neurosciences.

[1] Abbreviations: G-proteins, heterotrimeric guanine nucleotide-binding proteins; RGS4, regulators of G-protein signaling; $G_{i\alpha1}$, Gα subunit of heterotrimeric G-proteins; $G_{i\alpha1}$−AlF_4^-, Gα subunit of heterotrimeric G-proteins complexed with Mg^{2+}, GDP, and AlF_4^- stabilized in the transition state for GTP hydrolysis; DTT, DL-1,4-dithiothreitol; GTP, guanosine triphosphate; GDP, guanosine diphosphate; NMR, nuclear magnetic resonance; 2D, two dimensional; 3D, three dimensional; HSQC, heteronuclear single-quantum coherence spectroscopy; HMQC, heteronuclear multiple-quantum coherence spectroscopy; TPPI, time-proportional phase incrementation; NOE, nuclear Overhauser effect; NOESY, nuclear Overhauser enhanced spectroscopy; COSY, correlated spectroscopy; HNHA, amide proton to nitrogen to CαH proton correlation; HNHB, amide proton to nitrogen to CβH proton correlation; CT-HCACO, constant time CαH proton to α-carbon to carbonyl correlation; HACAHB, CαH proton to α-carbon to CβH proton correlation.

10.1021/bi992760w CCC: $19.00
Published on Web 05/20/2000

upon GTP hydrolysis. In the active Gα−GTP−Mg^{2+} complex, switch II and switch III regions become well ordered due to ionic interactions between the two switch regions where the conformational change in switch I is associated with binding Mg^{2+}. The Gα surface that binds the Gβγ dimer contains switch I and switch II regions. As a result of the formation of the Gα−GTP−Mg^{2+} complex, modifications in the structure of the three switch regions facilitate dissociation of Gα from Gβγ. The released subunits are then available to interact with a variety of target proteins to elicit the desired response. Termination of the signal results when the process is reversed by the hydrolysis of GTP bound to Gα. The reassociation of Gα with Gβγ then occurs, which results in the inactivation of the G-protein. Therefore, the duration of the G-protein signal is directly dependent on the GTPase activity of the Gα protein.

Regulators of G-protein signaling (RGS) affect the intensity and duration of the G-protein signal cascade by binding to the active Gα−GTP−Mg^{2+} complex and inducing a 50-fold increase in the rate of GTP hydrolysis (for reviews see refs *9*−*13*). Conversely, RGS proteins have little to no affinity for the inactive Gα−GDP complex. Thus, RGS act as attenuators of the induced G-protein signal by increasing the rate of inactivation of the G-protein and termination of the signal. The RGS family contains more than 20 members where specificity for Gα subtypes has been demonstrated and is probably associated with subtle sequence differences (*8*, *14*). RGS proteins are widely expressed (*13*). At least one RGS protein is found in every organ where many tissues express multiple RGS proteins. Additionally, members of the RGS family have region-specific expression in the brain where RGS4[2] is perhaps the most widely distributed and highly expressed RGS subtype (*15*, *16*). The regulation of RGS expression suggests an adaptive response in the brain signal transduction pathway to compensate for desensitization and sensitization of G-protein-coupled receptor function since RGS expression has been correlated with a response to an induced seizure (*16*). In addition to response to neurotransmiters, RGS activity has been associated with a variety of cellular functions including prolifferation, differentiation, membrane trafficking, and embryonic development (*9*, *10*, *12*, *17*).

An X-ray structure of RGS4 bound to $G_{i\alpha1}$ (*8*), site-directed mutagenesis data (*18*−*20*), and biochemical studies (*17*, *21*) suggest a potential mechanism for the RGS-induced Gα hydrolysis of GTP. These results imply that RGS4 binds preferentially to the Gα−GTP−Mg^{2+} complex and stabilizes the transition state structure of the switch regions, stimulating the intrinsic GTPase activity. Verifying this proposed mechanism fundamentally requires obtaining structural information for both free $G_{i\alpha1}$ and RGS4. Extensive structural information is available for $G_{i\alpha1}$ in five conformations thought to mimic the various stages of $G_{i\alpha1}$ in the GTPase cycle (*5*−*8*). This permits a direct comparison of $G_{i\alpha1}$ in the complex with RGS4 with other $G_{i\alpha1}$ conformers. These comparisons indicate that $G_{i\alpha1}$ in the RGS4−$G_{i\alpha1}$ complex exhibits only a 0.6 Å rms difference with $G_{i\alpha1}$ in the $G_{i\alpha1}$−AlF_4^- X-ray structure, where $G_{i\alpha1}$ is complexed with Mg^{2+}, GDP, and AlF_4^- and is trapped in the transition state for GTP hydrolysis. Additionally, the RGS4−$G_{i\alpha1}$ X-ray structure indicates that RGS4 binding induces a decrease in the mobility of the switch regions where critical interactions occur between r-N82[3] from RGS4 with switch regions I and II of $G_{i\alpha1}$ and between a-T182 from $G_{i\alpha1}$ with a binding pocket on RGS4. The RGS4 residue r-N82 has been identified as critical for facilitating the intrinsic $G_{i\alpha1}$ GTPase activity presumably by stabilizing the switch regions and substrate binding (*19*, *20*). Similar changes in the switch regions are observed between the Gα−GTP−Mg^{2+} complex and the Gα−GDP complex (*2*). Since the functional result of RGS4 binding to $G_{i\alpha1}$ is to induce GTP hydrolysis, it is reasonable to anticipate that the conformational change upon complex formation primarily occurs in $G_{i\alpha1}$. Nevertheless, in the absence of a free RGS4 structure it is difficult to speculate on a conformational contribution for RGS4 in the complex and how this may contribute to the selectivity of RGS4 for the Gα−GTP−Mg^{2+} complex and the induced GTPase activity and corresponding signal termination. Toward this goal we have previously presented the nearly complete ^1H, ^{15}N, ^{13}C, and ^{13}CO resonance assignments and secondary structure for RGS4 (*22*), and in this paper, we present the determination of the high-resolution solution conformation of free RGS4.

MATERIALS AND METHODS

NMR Sample Preparation. Uniformly (>95%) ^{15}N- and $^{15}N/^{13}C$-labeled recombinant RGS4 (19.0 kDa, 166 amino acids, p*I* 7.3) was expressed in *Escherichia coli* and purified as described previously (*22*). The NMR samples contained 1 mM RGS4 in a buffer containing 50 mM potassium phosphate, 2 mM NaN_3, and 50 mM deuterated DTT, in either 90% H_2O/10% D_2O or 100% D_2O at pH 6.0.

NMR Data Collection. All spectra were recorded at 35 °C on a Bruker AMX-2 600 spectrometer using a gradient-enhanced triple-resonance $^1H/^{13}C/^{15}N$ probe. For spectra recorded in H_2O, water suppression was achieved with the WATERGATE sequence and water flip-back pulses (*23*, *24*). Quadrature detection in the indirectly detected dimensions was recorded with the States−TPPI hypercomplex phase increment (*25*). Spectra were collected with appropriate refocusing delays to allow for 0, 0 or −90, 180 phase correction.

The RGS4 structure is based on the following series of spectra: HNHA (*26*), HNHB (*27*), 3D long-range $^{13}C-^{13}C$ correlation (*28*), coupled CT-HCACO (*29*, *30*), HACAHB−COSY (*31*), and 3D ^{15}N- (*32*, *33*) and ^{13}C-edited NOESY (*34*, *35*) experiments. The ^{15}N-edited NOESY and ^{13}C-edited NOESY experiments were collected with 100 and 120 ms mixing times, respectively.

Spectra were processed using the NMRPipe software package (*36*) and analyzed with PIPP (*37*) on a Sun Ultra 10 workstation. When appropriate, data processing included a solvent filter, zero-padding data to a power of 2, linear predicting back one data point of indirectly acquired data to obtain zero phase corrections, and linear prediction of

[2] Numbering for RGS4 is from amino acid residue 1 for the 158-residue RGS core domain form with an N-terminal Met and a six-residue histidine tag at the C-terminus. For comparison to the full-length RGS4 sequence, add 46 to the NMR sequence.

[3] Sequence numbers of RGS4 residues are prefixed with "r-", and those of Gα are prefixed with "a-".

additional points for the indirectly acquired dimensions to increase resolution. Linear prediction by means of the mirror image technique was used only for constant-time experiments (*38*). In all cases data were processed with a skewed sine-bell apodization function, and one zero-filling was used in all dimensions.

Interproton Distance Restraints. The NOEs assigned from 3D ^{13}C-edited NOESY and 3D ^{15}N-edited NOESY experiments were classified into strong, medium, weak, and very weak, corresponding to interproton distance restraints of 1.8−2.7 Å (1.8−2.9 Å for NOEs involving NH protons), 1.8−3.3 Å (1.8−3.5 Å for NOEs involving NH protons), 1.8−5.0 Å, and 3.0−6.0 Å, respectively (*39*, *40*). Upper distance limits for distances involving methyl protons and nonstereospecifically assigned methylene protons were corrected appropriately for center averaging (*41*).

Torsion Angle Restraints and Stereospecific Assignments. The β-methylene stereospecific assignments and χ_1 torsion angle restraints were obtained primarily from a qualitative estimate of the magnitude of $^3J_{\alpha\beta}$ coupling constants from the HACAHB−COSY experiment (*31*) and $^3J_{N\beta}$ coupling constants from the HNHB experiment (*27*). Further support for the assignments was obtained from approximate distance restraints for intraresidue NOEs involving NH, CαH, and CβH protons (*42*).

The ϕ and ψ torsion angle restraints were obtained from $^3J_{NH\alpha}$ coupling constants measured from the relative intensity of Hα cross-peaks to the NH diagonal in the HNHA experiment (*26*), from chemical shift analysis using the TALOS program (*43*), and from consistency with distance restraints for intraresidue and sequential NOEs involving NH, CαH, and CβH protons. $^1J_{C\alpha H\alpha}$ coupling constants obtained from a coupled 3D CT-HCACO spectrum were used to ascertain the presence of non-glycine residues with positive ϕ backbone torsion angles (*30*). The presence of a $^1J_{C\alpha H\alpha}$ coupling constant greater than 130 Hz allowed for a minimum ϕ restraint of −2° to −178°.

The Ile and Leu χ_2 torsion angle restraints and the stereospecific assignments for leucine methyl groups were determined from $^3J_{C\alpha C\delta}$ coupling constants obtained from the relative intensity of Cα and Cδ cross-peaks in a 3D long-range ^{13}C−^{13}C NMR correlation spectrum (*44*), in conjunction with the relative intensities of intraresidue NOEs (*45*). Stereospecific assignments for valine methyl groups were determined on the basis of the relative intensity of intraresidue NH−CγH and CαH−CγH NOEs as described by Zuiderweg et al. (*46*). The minimum ranges employed for the ϕ, ψ, and χ torsion angle restraints were ± 30°, ± 50°, and ± 20°, respectively (*47*).

Structure Calculations. The structures were calculated using the hybrid distance geometry−dynamical simulated annealing method of Nilges et al. (*48*) with minor modifications (*49*) using the program X-PLOR (*50*), adapted to incorporate pseudopotentials for $^3J_{NH\alpha}$ coupling constants (*51*), secondary ^{13}Cα/^{13}Cβ chemical shift restraints (*52*), and a conformational database potential (*53*, *54*). The target function that is minimized during restrained minimization and simulated annealing comprises only quadratic harmonic terms for covalent geometry, $^3J_{NH\alpha}$ coupling constants and secondary ^{13}Cα/^{13}Cβ chemical shift restraints, square-well quadratic potentials for the experimental distance and torsion angle restraints, and a quartic van der Waals term for nonbonded contacts. All peptide bonds were constrained to be planar and trans. There were no hydrogen-bonding, electrostatic, or 6-12 Lennard-Jones empirical potential energy terms in the target function.

Analysis of the a-T182 Binding Site on RGS4. The overall appearance of the NMR structure in the area of the proposed a-T182 binding site is one of greater size and accessibility. To obtain a more quantitative measurement of the differences in accessibility between the free RGS4 NMR structure and the X-ray structure of the RGS4−$G_{i\alpha1}$ complex, MOLCAD surfaces were calculated for both structures, and the surface area of each was measured.

The X-ray structure of the RGS4−$G_{i\alpha1}$ complex (AGR1) was read into SYBYL (Tripos), and all substructures except chain E (RGS4) were deleted. Additionally, all waters were deleted. Polar hydrogens were added and optimized using the Kollman united atom force field. This was followed by addition of all of the remaining hydrogens. MOLCAD was then used to generate a surface for all residues thought to be involved in binding of a-T182. These residues include r-I21, r-I27, r-F30, r-F33, r-L34, r-E37, r-S39, r-N42, r-I43, r-W46, r-I110, r-L113, r-M114, r-D117, r-S118, and r-R121. The surface area was calculated on the basis of the MOLCAD surface. MOLCAD was also used to calculate the surface area for the identical residues of the free RGS4 NMR structure. The surface area for the free RGS4 NMR structure was calculated to be 404.56 Å^2. The surface area for the crystal structure was calculated to be 321.88 Å^2. The difference in surface area of 82.67 Å^2 is an approximate 20% change in surface area between the two structures. A MOLCAD surface generated on the methyl and hydroxyl groups of a-T182 has a surface area of 57.72 Å^2.

RESULTS

Secondary Structure Analysis. The regular secondary structure elements of free RGS4 were identified from a qualitative analysis of sequential and interstrand NOEs, NH exchange rates, $^3J_{HN\alpha}$ coupling constants, and the ^{13}Cα and ^{13}Cβ secondary chemical shifts (*55*, *56*). The sequential and medium-range NOEs were obtained from a qualitative analysis of the ^{15}N-edited NOESY and ^{13}C-edited NOESY spectra. $^3J_{HN\alpha}$ coupling constants were obtained from the relative intensity of Hα cross-peaks to the NH diagonal in the HNHA experiment (*26*). Slowly exchanging NH protons were identified by recording an HSQC spectrum 2 h after exchanging an RGS4 sample from H_2O to D_2O. These data, together with the deduced secondary structure elements, are summarized in Figure 1. The overall structure of RGS4 is composed of seven helical regions corresponding to residues Q7−K12 (α_1), L17−S36 (α_2), E40−K53 (α_3), L61−E71 (α_4), C86−M95 (α_5), E105−S125 (α_6), and Y128−T132 (α_7).

Structure Determination. The final 30 simulated annealing structures were calculated on the basis of 2871 experimental NMR restraints consisting of 1960 approximate interproton distance restraints, 78 distance restraints for 39 backbone hydrogen bonds, 431 torsion angle restraints comprised of 151 ϕ, 154 ψ, 97 χ_1, and 29 χ_2 torsion angle restraints, 132 $^3J_{NH\alpha}$ restraints, and 136 Cα and 134 Cβ chemical shift restraints. Stereospecific assignments were obtained for 58 of the 125 residues with β-methylene protons, for the methyl

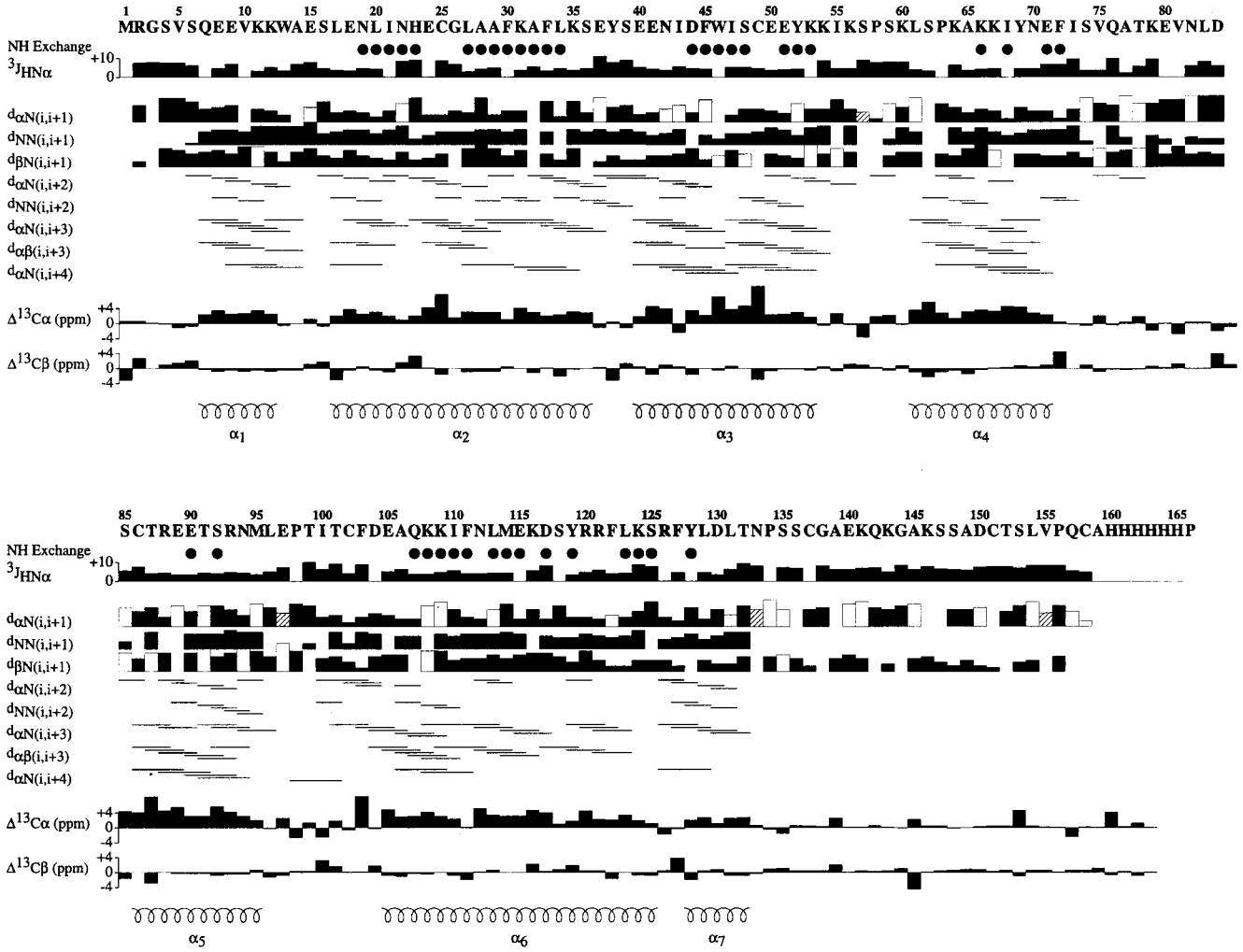

FIGURE 1: Summary of the sequential and medium-range NOEs involving the NH, Hα, and Hβ protons, the amide exchange and $^3J_{HN\alpha}$ coupling constant data, and the $^{13}C\alpha$ and $^{13}C\beta$ secondary chemical shifts observed for RGS4 with the secondary structure deduced from these data. The thickness of the lines reflects the strength of the NOEs. Amide protons still present after exchange to D_2O are indicated by closed circles. The open boxes represent potential sequential assignment NOEs which are obscured by resonance overlap and could therefore not be assigned unambiguously. The hashed boxes on the same line as the H$\alpha(i)-$NH$(i+1)$ NOEs represent the sequential NOE between the Hα proton of residue i and the CδH proton of the $i+1$ proline and are indicative of a trans proline.

groups of 3 of the 5 Val residues, and for the methyl groups of 9 of the 12 Leu residues. In addition, 7 out of the 8 Phe residues and 4 out of the 5 Tyr residues were well defined, making it possible to assign NOE restraints to only one of the pair of CδH and CϵH protons and to assign a χ_2 torsion angle restraint. A summary of the structural statistics for the final 30 simulated annealing (SA) structures of RGS4 is provided in Table 1, and a best fit superposition of the backbone atoms and selected side chains is shown in Figure 2. The atomic rms distribution of the 30 simulated annealing structures about the mean coordinate positions for residues 5−133 is 0.47 ± 0.05 Å for the backbone atoms, 0.86 ± 0.05 Å for all atoms, and 0.56 ± 0.04 Å for all atoms excluding disordered surface side chains (Table 1). The high quality of the RGS4 NMR structure is also evident by the results of PROCHECK analysis and by a calculated, large negative value for the Lennard-Jones van der Waals energy (−609 ± 11 kcal mol^{-1}). For the PROCHECK statistics, an overall *G*-factor of 0.25 ± 0.02, a hydrogen bond energy of 1.01 ± 0.04, and only 5.9 ± 2.4 bad contacts per 100 residues are consistent with a good quality structure comparable to an ∼1 Å X-ray structure. Additionally, most of the backbone torsion angles for non-glycine residues lie within expected regions of the Ramachandran plot where 94.3% of the residues lie within the most favored region of the Ramachandran ϕ, ψ plot and 5.7% in the additionally allowed region. $^1J_{C\alpha H\alpha}$ coupling constants from the coupled CT-HCACO experiment indicated that all non-glycine residues except Y38 have negative ϕ torsion angles.

DISCUSSION

Description of the RGS4 NMR Structure. A ribbon diagram of the restrained minimized average NMR structure of RGS4 is depicted in Figure 3B. A simple description of the RGS4 topology is of a protein that consists of two pseudo-right-handed four-helix bundles with an up−down−up−down arrangement where helical region 6 is part of both bundles. An unusual feature of the RGS4 structure occurs in the second helical region. There is a one-residue (H23) ∼90° bend in the helix which effectively divides this helical region into two separate helices [as described in the RGS4 X-ray structure (*8*)]. This one-residue bend was not obvious from the NMR analysis of the secondary structure data (Figure 1) where it appears to be a continual helical stretch. The

Table 1: Structural Statistics and Atomic rms Differences[a]

(A) Structural Statistics

	⟨SA⟩	$(\overline{SA})_r$	X-ray[b]
rmsd from exptl distance restraints (Å)[c]			
all (2038)	0.015 ± 0.002	0.014	0.311
interresidue sequential ($\|i-j\|=1$) (611)	0.013 ± 0.003	0.013	0.162
interresidue short range ($1<\|i-j\|\le 5$) (540)	0.013 ± 0.004	0.009	0.396
interresidue long range ($\|i-j\|>5$) (349)	0.020 ± 0.004	0.024	0.467
intraresidue (460)	0.011 ± 0.005	0.004	0.165
H-bonds (78)[d]	0.021 ± 0.008	0.024	0.181
rmsd from exptl dihedral restraints (deg) (431)[c,e]	0.101 ± 0.058	0.139	30.7
rmsd from exptl Cα restraints (ppm) (136)	1.03 ± 0.03	1.00	1.18
rmsd from exptl Cβ restraints (ppm) (134)	0.82 ± 0.06	0.74	0.77
rmsd from $^3J_{NH\alpha}$ restraints (Hz) (132)	0.62 ± 0.04	0.66	1.62
F_{NOE} (kcal mol^{-1})[f]	22.2 ± 6.7	19.4	9417
F_{tor} (kcal mol^{-1})[f]	0.30 ± 0.34	0.42	20576
F_{repel} (kcal mol^{-1})[f]	38.0 ± 3.3	28.3	1658
F_{L-J} (kcal mol^{-1})[g]	−609 ± 11	−585	−5
deviations from idealized covalent geometry			
bonds (Å) (2149)	0.003 ± 0	0.002	0.047
angles (deg) (3885)	0.454 ± 0.010	0.396	2.454
impropers (deg) (1109)[h]	0.442 ± 0.0303	0.351	28.33
PROCHECK[i]			
overall *G*-factor	0.25 ± 0.02	0.25	−1.04
% residues in most favorable region of Ramachandran plot	94.5 ± 1.0	94.3	86.1
H-bond energy	1.01 ± 0.04	0.90	0.70
no. of bad contacts/100 residues	5.9 ± 2.4	3.1	0.8

(B) Atomic rms Differences (Å)

	residues 5−133		secondary structure[j]		ordered side chain[k]
	backbone atoms	all atoms	backbone atoms	all atoms	all atoms
⟨SA⟩ vs $\overline{SA}$	0.47 ± 0.05	0.86 ± 0.05	0.44 ± 0.05	0.84 ± 0.05	0.56 ± 0.04
⟨SA⟩ vs $(\overline{SA})_r$	0.50 ± 0.04	0.97 ± 0.06	0.47 ± 0.05	0.95 ± 0.06	0.60 ± 0.04
$(\overline{SA})_r$ vs $\overline{SA}$	0.16	0.44	0.17	0.44	0.22
$\overline{SA}$ vs X-ray	1.94	2.33	1.60	2.05	2.14
$(\overline{SA})_r$ vs X-ray	1.94	2.38	1.61	2.13	2.15
⟨SA⟩ vs X-ray	1.99 ± 0.11	2.48 ± 0.11	1.65 ± 0.11	2.22 ± 0.10	2.21 ± 0.12

[a] The notation of the structures is as follows: ⟨SA⟩ are the final 30 simulated annealing structures, $\overline{SA}$ is the mean structure obtained by averaging the coordinates of the individual SA structures best fit to each other (excluding residues 1−4 and 134−166), and $(\overline{SA})_r$ is the restrained minimized mean structure (residues 5−133) obtained by restrained minimization of the mean structure $\overline{SA}$ (*58*). The number of terms for the various restraints is given in parentheses. [b] X-ray is the 2.8 Å resolution X-ray structure of Tesmer et al. (*8*). Tyr and Phe χ_2 dihedral angles in the X-ray structure were changed to be consistent with the NMR structure since it is not possible to differentiate between +90° or −90° in the X-ray structure. Without this correction, the calculation of F_{NOE} and F_{tor} would be artificially high for the X-ray structure. Residues 1−4 and 133−166 are not present in the X-ray structure. [c] None of the structures exhibited distance violations greater than 0.1 Å or dihedral angle violations greater than 1°. [d] For backbone NH−CO hydrogen bonds there are two restraints: r_{NH-O} = 1.5−2.3 Å and r_{N-O} = 2.5−3.3 Å. All hydrogen bonds involve slowly exchanging NH protons. [e] The torsion angle restraints comprise 151 ϕ, 154 ψ, 97 χ_1, and 29 χ_2 restraints. [f] The values of the square-well NOE (F_{NOE}) and torsion angle (F_{tor}) potentials [cf. eqs 2 and 3 in Clore et al. (*40*)] are calculated with force constants of 50 kcal mol^{-1} Å^{-2} and 200 kcal mol^{-1} rad^{-2}, respectively. The value of the quartic van der Waals repulsion term (F_{rep}) [cf. eq 5 in Nilges et al. (*48*)] is calculated with a force constant of 4 kcal mol^{-1} Å^{-4} with the hard-sphere van der Waals radius set to 0.8 times the standard values used in the CHARMM (*59*) empirical energy function (*48*, *58*, *60*). [g] E_{L-J} is the Lennard-Jones van der Waals energy calculated with the CHARMM empirical energy function and is *not* included in the target function for simulated annealing or restrained minimization. [h] The improper torsion restraints serve to maintain planarity and chirality. [i] These were calculated using the PROCHECK program (*61*). [j] The residues in the regular secondary structure are 7−12 (α_1), 17−36 (α_2), 40−53 (α_3), 61−71 (α_4), 86−95 (α_5), 105−125 (α_6), and 128−132 (α_7). [k] The disordered side chains that were excluded are as follows: residues 1−4; residues 134−166; Gln 7 from Cδ; Glu 8 from Cδ; Glu 9 from Cδ; Lys 11 from Cδ; Lys 12 from Cϵ; Glu 15 from Cδ; Glu 18 beyond Cγ; Asn 19 beyond Cβ; Ile 21 beyond Cβ; Asn 22 beyond Cβ; Glu 24 from Cδ; Lys 31 beyond Cϵ; Lys 35 from Cγ; Glu 37 beyond Cγ; Ser 39 beyond Cβ; Glu 40 beyond Cγ; Glu 41 beyond Cγ; Asn 42 beyond Cγ; Cys 49 beyond Cβ; Glu 50 from Cδ; Glu 51 beyond Cδ; Lys 53 beyond Cϵ; Lys 54 beyond Cϵ; Lys 56 beyond Cϵ; Ser 59 beyond Cβ; Lys 60 from Cϵ; Lys 64 beyond Cϵ; Lys 66 beyond Cϵ; Lys 67 beyond Cϵ; Glu 71 beyond Cδ; Ser 74 beyond Cβ; Gln 76 beyond Cδ; Lys 79 beyond Cϵ; Glu 80 beyond Cδ; Asp 84 from Cγ; Ser 85 beyond Cβ; Cys 86 beyond Cβ; Arg 88 from Cζ; Glu 89 beyond Cδ; Glu 90 beyond Cδ; Arg 93 from Cζ; Asn 94 beyond Cγ; Met 95 beyond Cγ; Glu 97 from Cγ; Asp 104 beyond Cγ; Glu 105 from Cδ; Gln 107 beyond Cδ; Lys 108 beyond Cϵ; Lys 109 beyond Cϵ; Asn 112 beyond Cγ; Leu 113 beyond Cγ; Glu 115 beyond Cδ; Lys 116 from Cγ; Asp 117 from Cγ; Arg 120 from Cδ; Arg 121 from Cδ; Lys 124 beyond Cϵ; Ser 125 beyond Cβ; Arg 126 from Cγ; Asp 130 beyond Cγ; Asn 133 from Cβ

bend only became apparent during the structure refinement process. Some observable NOEs that contribute to the bend at H23 occur between residues L20, I21 and residues G26, L27, A29, and F30. The bend at H23 effectively allows for appropriate packing of these hydrophobic side chains.

Additional bends or turns occur throughout the RGS4 structure. Helical regions α_1 and α_2 are connected by residue S16 that adopts an extended conformation, allowing these two helices to be essentially parallel. This is very similar to the turns connecting helical regions α_3 and α_4 and helical regions α_5 and α_6. Conversely, helical regions α_2 and α_3 are connected by Y38 that has a positive ϕ torsion angle, suggesting a β-type turn. The conformation of Y38 results in an angle between helical regions α_2 and α_3 of ~45°, which also represents a transition point between the two pseudo-four-helix bundles. The longest loop in the structure occurs

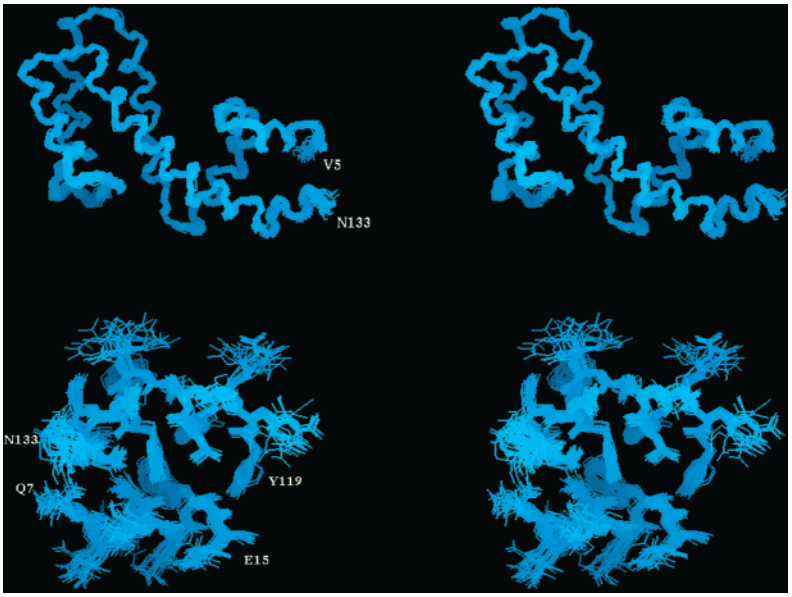

FIGURE 2: Stereoviews showing the best fit superposition of (A, top) the backbone (N, Cα, CO) and (B, bottom) all atoms of the 30 final simulated annealing structures for free RGS4. Residues V5−N133 and residues Q7−E15 and Y119−N133 are shown in panels A and B, respectively.

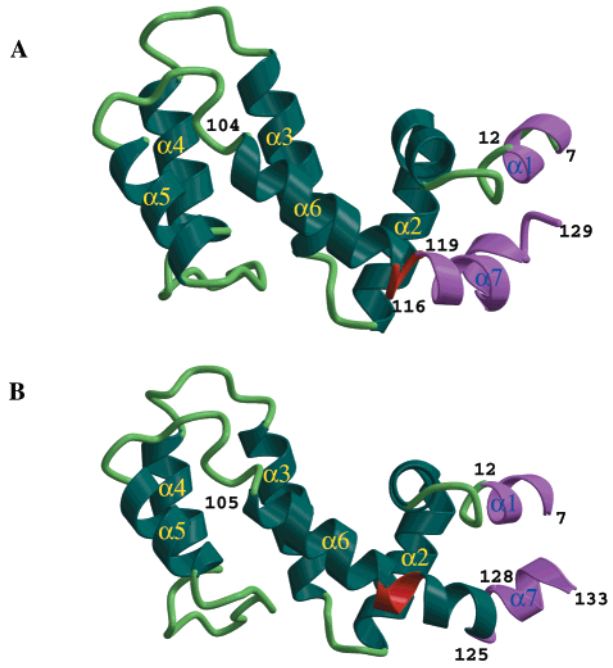

FIGURE 3: Ribbon diagrams of the (A) X-ray structure of RGS4 from the RGS4− $G_{i\alpha1}$ complex and (B) NMR structure of free RGS4 for residues r-V5 to r-P134. The residues that incur a significant structural change between the RGS4−$G_{i\alpha1}$ X-ray structure and the free RGS4 NMR structure are numbered. Residues r-K116 to r-Y119 which correspond to key residues involved in the interaction of $G_{i\alpha1}$ and the location of a structural change between the bound and free forms of RGS4 are colored red. The C- and N-terminal regions which incur a change in secondary structure and helical packing are colored pink. The observed helical regions for the RGS4 structures are labeled. The RGS4−$G_{i\alpha1}$ X-ray structure is that of Tesmer et al. (*8*).

between helical regions α_4 and α_5. This loop region is well ordered on the basis of high order parameters ($S^2 > 0.6$; data not shown). The low mobility for this loop results from interactions with helical regions α_3 and α_6. The observed bend between the longest helical region α_6 and the shortest helical region α_7 is suggestive of a distortion in this helical segment to achieve an optimal packing interaction between helical regions α_1 and α_7. The end result of these local conformations on the overall topology of RGS4 is to create an elongated structure where the two pseudo-four-helix bundles are nearly perpendicular. The interface between these two pseudo-four-helix bundles is predominately hydrophobic in nature (L17, I21, L27, F30, L34, W46, I47, I110, F111, L113, M114), consistent with the general packing of hydrophobic residues in the core of the protein with charged residues on the protein surface.

Another feature of the RGS4 structure is the observation that residues M1−S4 and P134−H166 are completely disordered and dynamically flexible. This is evident by the sharp line widths and the minimal number of observable NOEs. The flexible nature of these residues is further supported from ^{15}N T_1, T_2 and NOE measurements which indicate low-order parameters ($S^2 < 0.6$; data not shown).

As previously described, the primary biological function for RGS4 is to bind $G_{i\alpha1}$ and stimulate its intrinsic GTPase activity. Key residues in the RGS4 structure that are involved in the interaction of RGS4 with $G_{i\alpha1}$ correspond to RGS4 residues r-S39, r-E41, r-N42, r-L113, r-D117, r-S118, and r-R121 that form the binding pocket for a-T182 from $G_{i\alpha1}$. Similarly, r-N82 from RGS4 binds into the $G_{i\alpha1}$ active site, interacting with residues a-Q204, a-S206, and a-E207 (*8*). RGS4 mutational work supports the functional importance of these residues in the binding and activity of RGS4 with $G_{i\alpha1}$ while identifying r-N82 to be critical in facilitating GTP hydrolysis (*18*−*20*). RGS4 residues r-S39, r-E41, and r-N42 are located in the N-terminal end of helical region α_3 while r-L113, r-D117, r-S118, and r-R121 are located directly opposite at the C-terminal end of helical region α_6. r-N82 is located approximately in the center of the structured loop region between helical regions α_4 and α_5, which is positioned relatively above the a-T182 binding pocket on RGS4.

Comparison of the Free RGS4 NMR Structure with the RGS4 $G_{i\alpha1}$-Bound Structure. A common paradigm in describing a mechanism behind a biochemical process involving protein−protein interactions is to invoke an induced con-

formational change in the protein target. The resulting structural change in the protein is used to explain a modification in its enzymatic activity or affinity with another protein in the biological system. This is a familiar feature in the cascade of steps associated with signal transduction pathways. Nevertheless, direct structural evidence from NMR or X-ray data illustrating the proposed conformational change is rarely available. The obvious value in obtaining such structural information is to provide specific details of the induced conformational change to truly understand the biochemical process. The analysis of the G-protein signal transduction pathway is relatively unique in this respect because of the extensive structural information available for $G_{i\alpha1}$ during the various stages of the GTPase cycle (*2*−*5*). The observed structural changes for the various $G_{i\alpha1}$ conformers provide a fundamental understanding of the GTPase cycle and the mechanism for the signal cascade where RGS4 plays a critical role in signal termination. RGS4 has been identified as an attenuator of the G-protein signal cascade by binding specifically to the $G_{i\alpha1}$−GTP−Mg^{2+} complex and increasing the rate of GTP hydrolysis. The observed selectivity of RGS4 for the Gα−GTP−Mg^{2+} complex relative to the Gα−GDP complex is not readily apparent given the close similarity in these structures. Understanding the role of RGS4 in the G-protein signal cascade and particularly its activity and selectivity fundamentally requires obtaining structural information for RGS4 in both the free and bound forms. An unexpected result from determining the solution structure of RGS4 in the absence of $G_{i\alpha1}$ was the observation of a significant conformational change between the free and bound forms of RGS4 (*8*) (Figure 3).

A fundamental factor in the difference between the free and bound RGS4 structures is a perturbation in the secondary structure elements. Consistent with the RGS4−$G_{i\alpha1}$ X-ray structure, the NMR structure of free RGS4 is an α-helical protein comprised of two pseudo-four-helix bundles. The NMR data clearly indicate that the free RGS4 NMR structure is composed of seven helical regions where a majority of these data are consistent with the bound RGS4−$G_{i\alpha1}$ X-ray structure. The significant difference in the secondary structure between the $G_{i\alpha1}$-bound form of RGS4 and the free form of RGS4 occurs within the C-terminal helical regions α_6 and α_7. The bound RGS4−$G_{i\alpha1}$ X-ray structure indicates that residues r-D104−r-K116 and r-Y119−r-L129 are helical, where only residues r-V5−r-T132 are observed in the bound X-ray structure. This contrasts with the free RGS4 NMR structure where residues r-E105−r-S125 (α_6) and r-Y128−r-T132 (α_7) are helical and residues r-M1−r-S4 and r-P134−r-H166 are disordered.

A simple view of the observed structural change between the free RGS4 NMR structure and the bound RGS4−$G_{i\alpha1}$ X-ray structure is a movement of a kink between helical regions α_6 and α_7 toward the C-terminus. The movement of this kink results in α_6 being longer by nine residues and in α_7 being shorter by six residues in the free RGS4 NMR structure. Additionally, α_7 extends three residues beyond what was observed as a structural region in the bound RGS4−$G_{i\alpha1}$ X-ray structure. This observed change in the secondary structure definition for a few C-terminal residues has far-reaching effects. A significant modification in the overall fold for RGS4 results, which is evident by the 1.94 Å backbone rms difference between the bound RGS4−$G_{i\alpha1}$ X-ray structure and the free RGS4 NMR structure for residues r-V5−r-P134. The major effect of the alteration in secondary structures is a reorganization of the packing of the N-terminal and C-terminal helices. The repacking of the terminal helices is evident by the per-residue backbone atomic rms differences between the free RGS4 NMR structure and the bound RGS4−$G_{i\alpha1}$ X-ray structure (Figure 4). The backbone rms difference between the free and bound RGS4 structures is based on the superposition of the backbone atoms for r-V5−r-P134.

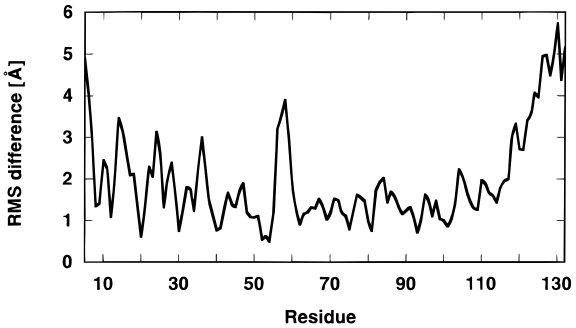

FIGURE 4: Backbone (N, Cα, CO) atomic rms differences between the free RGS4 NMR structure and the bound RGS4 X-ray structure as a function of residue number. The superposition of the structures was based on the backbone atoms of residues r-V5−r-P134.

The significant difference between the N- and C-terminal regions of the free RGS4 NMR structure and the bound RGS4−$G_{i\alpha1}$ X-ray structure is indicated by the large number of interproton distance (145) and torsion angle (39) violations and by the corresponding very high values for the NOE and torsion angle restraint energies exhibited by the bound RGS4−$G_{i\alpha1}$ X-ray structure (Table 2). From the self-consistency of the NMR data using NOEs, coupling constants, NH exchange rates, and secondary carbon chemical shifts and from the large number of restraint violations with the bound structure, it appears that the observed difference between the free RGS4 NMR structure and the bound RGS4−$G_{i\alpha1}$ X-ray structure is an actual portrayal of the effect of RGS4 binding $G_{i\alpha1}$.

Relevance to Activity for the RGS4 Conformational Change. RGS4 is involved in the regulation of the $G_{i\alpha1}$ GTPase cycle where it has a modest affinity for the Gα−GTP−Mg^{2+} complex and does not bind the Gα−GDP complex. Therefore, the observed conformational change for free RGS4 may be related to modulating its affinity to $G_{i\alpha1}$ to allow for perpetuation of the GTPase cycle. This role for the RGS4 conformational change is evident by the fact that the $G_{i\alpha1}$ binding site on RGS4 correlates with the location of the $G_{i\alpha1}$-induced structural perturbation. The pronounced kink between helical regions α_6 and α_7 observed in the bound RGS4−$G_{i\alpha1}$ X-ray structure occurs at residues r-D117 and r-S118. An expanded view of the RGS4 molecular surface for both the free RGS4 NMR structure and the bound RGS4−$G_{i\alpha1}$ X-ray structure in the vicinity of the a-T182 binding pocket on RGS4 is shown in Figure 5.

By visually comparing the RGS4 molecular surfaces, it is apparent that the a-T182 binding pocket on RGS4 is larger and more accessible in the free RGS4 NMR structure (Figure 5A,B). The size and accessibility of the a-T182 binding pocket on RGS4 are further exemplified by the observed increase in the surface area for the binding pocket from 404.56 to 321.88 $Å^2$ for the free and bound forms of RGS4,

Table 2: Number of Violations Exhibited by the X-ray Structure of RGS4−$G_{i\alpha1}$ with Respect to the Experimental NMR Interproton Distance and Torsion Angle Restraints[a]

	(A) Number of Violations in Interproton Distance Restraints					
	0.1−0.3 Å	0.3−0.5 Å	0.5−1.0 Å	1.0−2.0 Å	2.0−5.0 Å	>5.0 Å
all (2038)	41	19	41	28	16	0
interresidue sequential ($\|i-j\|=1$) (611)	<16	12	11	0	1	0
interresidue short range ($1<\|i-j\|\leq 5$) (540)	11	3	9	11	7	0
interresidue long range ($\|i-j\|>5$) (349)	4	3	15	14	7	0
intraresidue (460)	10	1	5	2	1	0
H-bonds (78)	0	0	1	1	0	0

	(B) Violations in Torsion Angle Restraints			
	10−30°	30−60°	60−120°	>120°
all (431)	6	0	31	2
ϕ (151)	2	0	0	0
ψ (154)	0	0	0	0
χ_1 (97)	2	0	28	2
χ_2 (29)	2	0	3	0

[a] The X-ray structure of RGS4 is the 2.8 Å resolution X-ray structure of Tesmer et al. (*8*). Residues r-M1−r-S4 and r-N133−r-H166 are not present in the X-ray structure. The total number of interproton distance and torsion angle restraints in each category is given in parentheses. Tyr and Phe χ_2 dihedral angles in the X-ray structure were changed to be consistent with the NMR structure since it is not possible to differentiate between +90° or −90° in the X-ray structure. Without this correction, the number of violations would be artificially high for the X-ray structure.

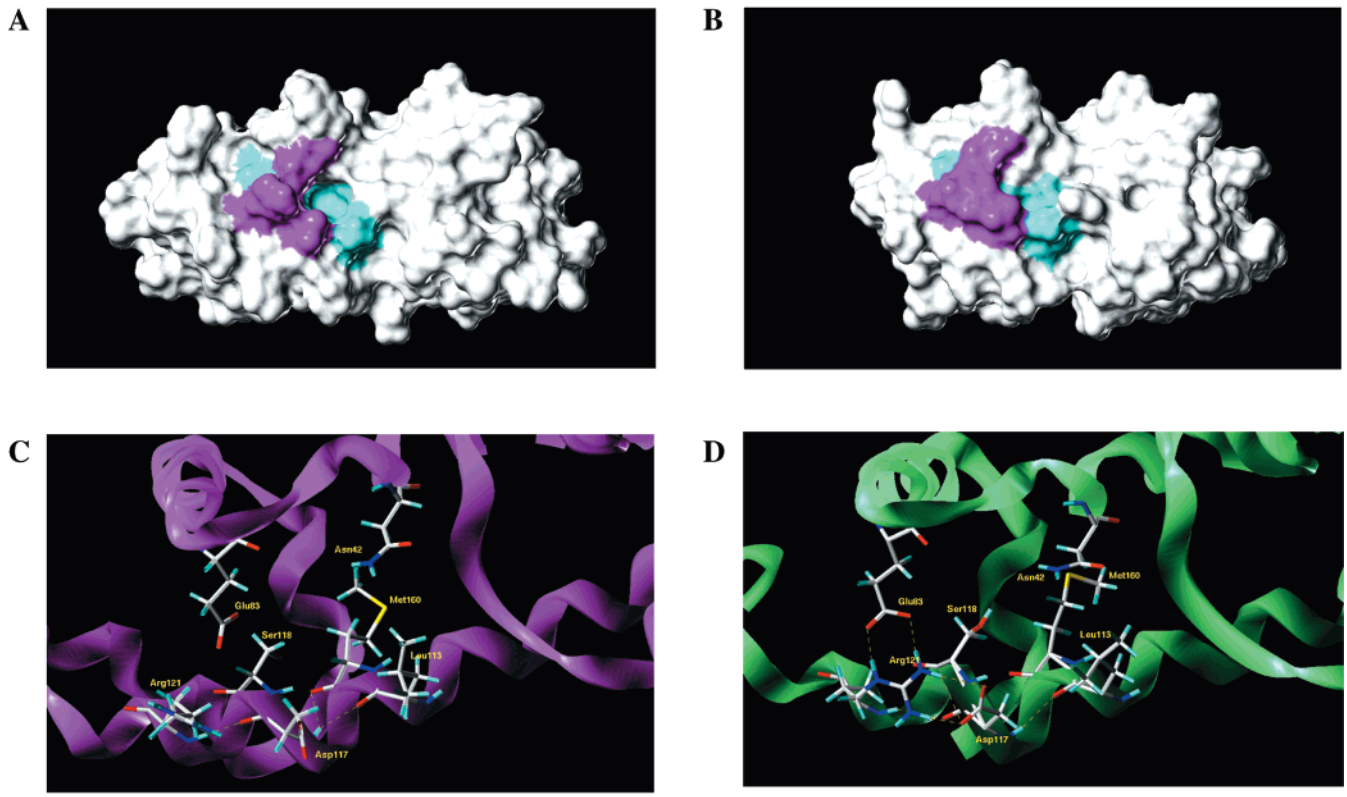

FIGURE 5: Molecular surface of (A) the free RGS4 NMR structure and (B) the RGS4−$G_{i\alpha1}$ X-ray structure with the side chains for r-D117, r-S118, and r-R121 colored blue and the a-T182 binding pocket colored magenta. Stick and ribbon representation of the expanded view of (C) the free RGS4 NMR structure and (D) the RGS4−$G_{i\alpha1}$ X-ray structure centered on the a-T182 binding pocket.

respectively. The observed 82.67 Å^2 change in the a-T182 binding pocket corresponds to an approximate 20% increase in the surface area for the free RGS4 binding pocket. The binding surface area of a-T182 indicates the relative significance of this observed change in surface area. The surface area for the methyl and hydroxyl groups of a-T182 is 57.72 Å^2, which is significantly smaller than the observed change in the surface area between the free and bound RGS4 structures.

Also, in the bound RGS4−$G_{i\alpha1}$ X-ray structure there appears to be a molecular surface "wall" composed of the RGS4 side chains from residues r-D117, r-S118, and r-R121 which surround the a-T182 binding pocket on RGS4. These residues form an important hydrogen-bonding network which is critical for the binding of RGS4 with $G_{i\alpha1}$ where r-D117 forms a hydrogen bond with r-R121 and the backbone nitrogen of a-T182. This hydrogen-bonding network is effectively absent in the free RGS4 NMR structure. The side chains for r-D117, r-S118, and r-R121 are well beyond hydrogen-bonding distance in the free RGS4 NMR since the helical kink at residues r-D117 and r-S118 is less pronounced and the disruption in the helix occurs between residues r-S125−r-Y128. Thus, the greater accessibility of the a-T182 binding pocket on free RGS4 is suggested by the absence

of the salt bridges formed by r-E37, r-D117, and r-R121 as well as the movement of r-S118 away from the binding pocket. The relative positions of these side chains in both the bound RGS4−$G_{i\alpha1}$ X-ray structure and the free RGS4 NMR structure are depicted in panels C and D of Figure 5, respectively.

r-N82 has been identified as a critical residue on RGS4 for facilitating the intrinsic $G_{i\alpha1}$ GTPase activity (*8*, *18*−*20*). The key component of the r-N82 contributions to the RGS4 activity has been attributed to stabilization of $G_{i\alpha1}$ switch regions and substrate binding. Comparison of the free RGS4 NMR structure with the bound RGS4−$G_{i\alpha1}$ X-ray structure in the vicinity of r-N82 does not suggest a significant conformational change in this region of the protein when RGS4 binds $G_{i\alpha1}$ (Figure 4). The only observable change is seen for the side-chain conformation of r-N82. In the bound RGS4−$G_{i\alpha1}$ X-ray structure the side chain for r-N82 extends out from the RGS4 surface to effectively interact with $G_{i\alpha1}$. Conversely, the side chain for r-N82 points toward the a-T182 binding pocket. Since r-N82 is a surface- and solvent-exposed residue in the absence of $G_{i\alpha1}$, the side-chain conformation for r-N82 in the free RGS4 NMR structure does not appear to have any significant structural contributions and should readily adopt the bound conformation without any consequences.

The observation that RGS4 undergoes a significant structural change in the presence of $G_{i\alpha1}$ where the focal point of this change occurs at key residues in the RGS4−$G_{i\alpha1}$ interface creates a different picture for the process of RGS4 activation of the intrinsic $G_{i\alpha1}$ GTPase activity. A two-stage process composed of a binding and locking step is suggested from comparison of the free and bound forms of RGS4. The a-T182 binding pocket on RGS4 is clearly larger and more accessible in the free RGS4 NMR structure, suggestive of an "open" conformation (Figure 5A,B). This implies that the binding step may be driven by the ease of fit of a-T182 into the open conformation of the pocket. The locking step corresponds to an induced change in the RGS4 structure from the open binding pocket conformation to a "closed" conformation that effectively locks a-T182 into the RGS4 binding pocket. The locking mechanism is attributed to the formation of the hydrogen-bonding network observed in the RGS4−$G_{i\alpha1}$ X-ray structure where the pronounced kink occurs in the helix between residues r-D117 and r-S118 such that these residues are brought into close contact with r-R121 and a-T182. Thus the presence of a-T182 in the pocket induces the formation of the hydrogen-bonding network and the resulting RGS4 conformational change as opposed to the preformed binding site observed in the RGS4−$G_{i\alpha1}$ X-ray structure.

The release of RGS4 from $G_{i\alpha1}$ would then require the removal of a-T182 from the RGS4 binding pocket and the corresponding relaxation of the RGS4 structure to the open conformation seen in the free form of RGS4. This presumably occurs during GTP hydrolysis, which is consistent with the local perturbation in the vicinity of a-T182 seen between the $G_{i\alpha1}$−GDP (*5*) and RGS4−$G_{i\alpha1}$ X-ray structures (Figure 6). The structure for the $G_{i\alpha1}$−GDP complex illustrates the conformation of $G_{i\alpha1}$ upon completion of GTP hydrolysis. The localized movement of a-T182 appears to be sufficient to remove a-T182 from the RGS4 binding pocket and disrupt the hydrogen-bonding network, resulting in dissociation of the complex. Comparison of the a-T182 region between the RGS4−$G_{i\alpha1}$ and the $G_{i\alpha1}$−AlF_4^- X-ray structure indicates that these two structures are essentially identical in this region of $G_{i\alpha1}$ (*7*) (Figure 6). The $G_{i\alpha1}$−AlF_4^- X-ray structure corresponds to the conformation of $G_{i\alpha1}$ trapped in the transition state for GTP hydrolysis, which is the conformation that RGS4 preferentially binds (*17*, *21*, *57*). Thus, the observation that RGS4 undergoes a structural change upon preferential binding to $G_{i\alpha1}$ in a conformation consistent with the $G_{i\alpha1}$ GTP transition state is consistent with the proposed mechanism for the activity of RGS4 by stabilizing the GTP transition state of $G_{i\alpha1}$ (*8*, *17*−*21*).

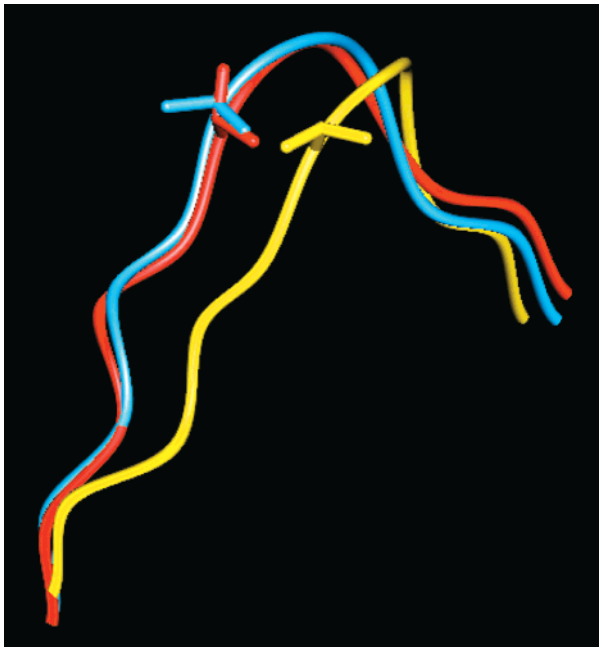

FIGURE 6: Overlay of the $G_{i\alpha1}$ backbone atoms for residues a-T177−a-T187 from the GDP−$G_{i\alpha1}$ (yellow) (*5*), RGS4−$G_{i\alpha1}$ (red) (*8*), and GDP−AlF_4^- $G_{i\alpha1}$ (blue) (*7*) X-ray structures in the vicinity of a-T182. Only the side chain for a-T182 is shown.

The similarity between the RGS4−$G_{i\alpha1}$ and the $G_{i\alpha1}$−AlF_4^- X-ray structures and the difference between these structures with $G_{i\alpha1}$−GDP also implies a mechanism for the selectivity of RGS4 for the $G_{i\alpha1}$−GTP−Mg^{2+} complex and a means to facilitate the GTPase cycle. The observed RGS4 selectivity for the $G_{i\alpha1}$−GTP−Mg^{2+} complex arises from the fundamental difference between a $G_{i\alpha1}$ structure complexed with either GDP or GTP and the critical requirement for the binding of a-T182 within the RGS4 binding pocket to induce the bound form of RGS4. Essentially, the formation of the RGS4−$G_{i\alpha1}$ complex now requires both the proper orientation of a-T182 and the presence of the bound form of RGS4. Since the orientation of a-T182 and the bound form of RGS4 is directly coupled and interdependent, a higher order of selectivity is achieved. It readily follows that efficient dissociation of the RGS4−$G_{i\alpha1}$ complex will follow GTP hydrolysis since a-T182 will no longer be in the proper binding conformation in the $G_{i\alpha1}$−GDP complex, resulting in the conversion of RGS4 to its free form.

Conclusion. The NMR solution structure of free RGS4 reveals the unexpected observation that the protein undergoes a significant conformational change upon binding $G_{i\alpha1}$. The focal point of this structural change occurs at key residues in the RGS4−$G_{i\alpha1}$ interface where the a-T182 binding pocket

is larger and more accessible, indicative of an open conformation. The RGS4 structural change is correlated with the binding of a-T182 into the RGS4 binding pocket with the subsequent formation of a hydrogen bond network, suggesting a two-step process composed of a binding and locking step. The induced RGS4 conformation in the presence of $G_{i\alpha1}$ suggests a mechanism for its selective binding to the $G_{i\alpha1}$−GTP−Mg^{2+} complex and the corresponding perpetuation of the GTPase cycle. The X-ray structures of various $G_{i\alpha1}$−guanine nucleotide complexes indicate a significant conformational change in the vicinity of a-T182 associated with GTPase activity. This observation implies that the successful complex formation between RGS4 and $G_{i\alpha1}$ is dependent on *both* the formation of the bound RGS4 conformation and the proper orientation of a-T182. Since the bound form of RGS4 and the proper orientation of a-T182 are intrinsically coupled, a higher order of selectivity is obtained for the binding of RGS4 with the $G_{i\alpha1}$−GTP−Mg^{2+} complex. Similarly, the release of RGS4 from $G_{i\alpha1}$ and the continuation of the GTPase cycle are facilitated by the combination of the a-T182 and RGS4 conformational changes. Additionally, since the conformation of a-T182 is identical in both the GTP hydrolysis transition state and the $G_{i\alpha1}$−GTP−Mg^{2+} complex, the RGS4 structural change is consistent with the proposed mechanism for RGS4 activity based on stabilizing the GTP hydrolysis transition state. Thus, the described structural change in RGS4 provides an elegant mechanism for the observed binding selectivity between the various Gα conformers despite the close similarity in these structures while supporting the proposed mechanism for RGS4 activity.

REFERENCES

1. Neer, E. J. (1995) *Cell 80*, 249−257.
2. Sprang, S. R. (1997) *Annu. Rev. Biochem. 66*, 639−678.
3. LeVine, H., III (1999) *Mol. Neurobiol. 19*, 111−149.
4. Farfel, Z., Bourne, H. R., and Iiri, T. (1999) *N. Engl. J. Med. 340*, 1012−1020.
5. Berghuis, A. M., Lee, E., Raw, A. S., and Gilman, A. (1996) *Structure 4*, 1277−1290.
6. Mixon, M. B., Lee, E., Coleman, D. E., and Berghuis, A. (1995) *Science 270*, 954−960.
7. Coleman, D. E., Berghuis, A. M., Lee, E., and Linder, M. E. (1994) *Science 265*, 1405−1412.
8. Tesmer, J. J. G., Berman, D. M., Gilman, A. G., and Sprang, S. R. (1997) *Cell 89*, 251−261.
9. Dohlman, H. G., and Thorner, J. (1997) *J. Biol. Chem. 272*, 3871−3874.
10. Kehrl, J. H. (1998) *Immunity 8*, 1−10.
11. Arshavsky, V. Y., and Pugh, E. N., Jr. (1998) *Neuron 20*, 11−14.
12. Zerangue, N., and Jan, L. Y. (1998) *Curr. Biol. 8*, R313−R316.
13. De Vries, L., and Farquhar, M. G. (1999) *Trends Cell Biol. 9*, 138−144.
14. Kozasa, T., Jiang, X., Hart, M. J., Sternweis, P. M., Singer, W. D., Gilman, A. G., Bollag, G., and Sternweis, P. C. (1998) *Science 280*, 2109−2112.
15. Nomoto, S., Adachi, K., Yang, L.-X., Hirata, Y., Muraguchi, S., and Kiuchi, K. (1997) *Biochem. Biophys. Res. Commun. 241*, 281−287.
16. Gold, S. J., Ni, Y. G., Dohlman, H. G., and Nestler, E. (1997) *J. Neurosci. 17*, 8024−8037.
17. Berman, D. M., Kozasa, T., and Gilman, A. G. (1996) *J. Biol. Chem. 271*, 27209−27212.
18. Srinivasa, S. P., Watson, N., Overton, M. C., and Blumer, K. J. (1998) *J. Biol. Chem. 273*, 1529−1533.
19. Posner, B. A., Mukhopadhyay, S., Tesmer, J. J., Gilman, A. G., and Ross, E. M. (1999) *Biochemistry 38*, 7773−7779.
20. Natochin, M., McEntaffer, R. L., and Artemyev, N. O. (1998) *J. Biol. Chem. 273*, 6731−6735.
21. Watson, N., Linder, M. E., and Druey, K. M. (1996) *Nature 383*, 172−175.
22. Moy, F., Chanda, P. K., Cockett, M. I., Edris, W., Jones, P. G., and Powers, R. (1999) *J. Biomol. NMR 15*, 339−340.
23. Piotto, M., Saudek, V., and Sklenar, V. (1992) *J. Biomol. NMR 2*, 661−665.
24. Grzesiek, S., and Bax, A. (1993) *J. Am. Chem. Soc. 115*, 12593−12594.
25. Marion, D., Ikura, M., Tschudin, R., and Bax, A. (1989) *J. Magn. Reson. 85*, 393−399.
26. Vuister, G. W., and Bax, A. (1993) *J. Am. Chem. Soc. 115*, 7772−7777.
27. Archer, S. J., Ikura, M., Torchia, D. A., and Bax, A. (1991) *J. Magn. Reson. 95*, 636−641.
28. Bax, A., and Pochapsky, S. S. (1992) *J. Magn. Reson. 99*, 638−643.
29. Powers, R., Gronenborn, A. M., Clore, G. M., and Bax, A. (1991) *J. Magn. Reson. 94*, 209−213.
30. Vuister, G. W., Delaglio, F., and Bax, A. (1992) *J. Am. Chem. Soc. 114*, 9674−9675.
31. Grzesiek, S., Kuboniwa, H., Hinck, A. P., and Bax, A. (1995) *J. Am. Chem. Soc. 117*, 5312−5315.
32. Marion, D., Driscoll, P. C., Kay, L. E., Wingfield, P. T., Bax, A., Gronenborn, A. M., and Clore, G. M. (1989) *Biochemistry 28*, 6150−6156.
33. Zuiderweg, E. R. P., and Fesik, S. W. (1989) *Biochemistry 28*, 2387−2391.
34. Zuiderweg, E. R. P., McIntosh, L. P., Dahlquist, F. W., and Fesik, S. W. (1990) *J. Magn. Reson. 86*, 210−216.
35. Ikura, M., Kay, L. E., Tschudin, R., and Bax, A. (1990) *J. Magn. Reson. 86*, 204−209.
36. Delaglio, F., Grzesiek, S., Vuister, G. W., Zhu, G., Pfeifer, J., and Bax, A. (1995) *J. Biomol. NMR 6*, 277−293.
37. Garrett, D. S., Powers, R., Gronenborn, A. M., and Clore, G. M. (1991) *J. Magn. Reson. 95*, 214−220.
38. Zhu, G., and Bax, A. (1992) *J. Magn. Reson. 100*, 202−207.
39. Williamson, M. P., Havel, T. F., and Wuethrich, K. (1985) *J. Mol. Biol. 182*, 295−315.
40. Clore, G. M., Nilges, M., Sukumaran, D. K., Bruenger, A. T., Karplus, M., and Gronenborn, A. M. (1986) *EMBO J. 5*, 2729−2735.
41. Wuthrich, K., Billeter, M., and Braun, W. (1983) *J. Mol. Biol. 169*, 949−961.
42. Powers, R., Garrett, D. S., March, C. J., Frieden, E. A., Gronenborn, A. M., and Clore, G. M. (1993) *Biochemistry 32*, 6744−6762.
43. Cornilescu, G., Delaglio, F., and Bax, A. (1999) *J. Biomol. NMR 13*, 289−302.
44. Bax, A., Max, D., and Zax, D. (1992) *J. Am. Chem. Soc. 114*, 6923−6925.
45. Powers, R., Garrett, D. S., March, C. J., Frieden, E. A., Gronenborn, A. M., and Clore, G. M. (1993) *Biochemistry 32*, 6744−6762.
46. Zuiderweg, E. R. P., Boelens, R., and Kaptein, R. (1985) *Biopolymers 24*, 601−611.
47. Kraulis, P. J., Clore, G. M., Nilges, M., Jones, T. A., Pettersson, G., Knowles, J., and Gronenborn, A. M. (1989) *Biochemistry 28*, 7241−7257.
48. Nilges, M., Gronenborn, A. M., Bruenger, A. T., and Clore, G. M. (1988) *Protein Eng. 2*, 27−38.
49. Clore, G. M., Appella, E., Yamada, M., Matsushima, K., and Gronenborn, A. M. (1990) *Biochemistry 29*, 1689−1696.
50. Brunger, A. T. (1993) *X-PLOR Version 3.1 Manual*, Yale University, New Haven, CT.
51. Garrett, D. S., Kuszewski, J., Hancock, T. J., Lodi, P. J., Vuister, G. W., Gronenborn, A. M., and Clore, G. M. (1994) *J. Magn. Reson., Ser. B 104*, 99−103.
52. Kuszewski, J., Qin, J., Gronenborn, A. M., and Clore, G. M. (1995) *J. Magn. Reson., Ser. B 106*, 92−96.

53. Kuszewski, J., Gronenborn, A. M., and Clore, G. M. (1996) *Protein Sci. 5*, 1067−1080.
54. Kuszewski, J., Gronenborn, A. M., and Clore, G. M. (1997) *J. Magn. Reson. 125*, 171−177.
55. Clore, G. M., and Gronenborn, A. M. (1989) *Crit. Rev. Biochem. Mol. Biol. 24*, 479−564.
56. Wishart, D. S., and Sykes, B. D. (1994) *Methods Enzymol. 239*.
57. Chen, C.-K., Wieland, T., and Simon, M. I. (1996) *Proc. Natl. Acad. Sci. U.S.A. 93*, 12885−12889.
58. Nilges, M., Clore, G. M., and Gronenborn, A. M. (1988) *FEBS Lett. 239*, 129−136.
59. Brooks, B. R., Bruccoleri, R. E., Olafson, B. D., States, D. J., Swaminathan, S., and Karplus, M. (1983) *J. Comput. Chem. 4*, 187−217.
60. Nilges, M., Clore, G. M., and Gronenborn, A. M. (1988) *FEBS Lett. 229*, 317−324.
61. Laskowski, R. A., MacArthur, M. W., Moss, D. S., and Thornton, J. M. (1993) *J. Appl. Crystallogr. 26*, 283−291.

BI992760W